UC San Diego
UC San Diego Previously Published Works

Title

A new non-canonical pathway of Gαq protein regulating mitochondrial dynamics and bioenergetics

Permalink

Journal

ISSN

Authors

Benincá, Cristiane
Planagumà, Jesús
de Freitas Shuck, Adriana
et al.

Publication Date
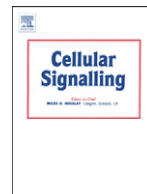
DOI

Peer reviewed

A new non-canonical pathway of Gα$_q$ protein regulating mitochondrial dynamics and bioenergetics

Cristiane Benincá [a,c], Jesús Planagumà [b,1], Adriana de Freitas Shuck [a], Rebeca Acín-Perez [c], Juan Pablo Muñoz [d,e,f], Marina Mateus de Almeida [g], Joan H. Brown [h], Anne N. Murphy [h], Antonio Zorzano [d,e,f], Jose Antonio Enríquez [c], Anna M. Aragay [a,b,*]

[a] Molecular Biology Institute of Barcelona (IBMB), Spanish National Research Council (CSIC), Barcelona 08028, Spain
[b] Department of Biomedicine, University of Bergen, 5009 Bergen, Norway
[c] Department of Cardiovascular Development and Repair, Spanish Cardiovascular Research Center (CNIC), Madrid 28029, Spain
[d] Institute for Research in Biomedicine (IRB), Barcelona 08028, Spain
[e] Department of Biochemistry and Molecular Biology, University of Barcelona, Barcelona 08028, Spain
[f] CIBERDEM, Barcelona 08028, Spain
[g] Department of Genetics, Federal University of Paraná (UFPR), Curitiba PO Box 19071, Brazil
[h] Department of Pharmacology, University of California (UCSD), San Diego, CA 92093-0636, USA

ARTICLE INFO

ABSTRACT

Contrary to previous assumptions, G proteins do not permanently reside on the plasma membrane, but are constantly monitoring the cytoplasmic surfaces of the plasma membrane and endomembranes. Here, we report that the Gα$_q$ and Gα$_{11}$ proteins locate at the mitochondria and play a role in a complex signaling pathway that regulates mitochondrial dynamics. Our results provide evidence for the presence of the heteromeric G protein (Gα$_{q/11}$βγ) at the outer mitochondrial membrane and for Gα$_q$ at the inner membrane. Both localizations are necessary to maintain the proper equilibrium between fusion and fission; which is achieved by altering the activity of mitofusin proteins, Drp1, OPA1 and the membrane potential at both the outer and inner mitochondrial membranes. As a result of the absence of Gα$_{q/11}$, there is a decrease in mitochondrial fusion rates and a decrease in overall respiratory capacity, ATP production and OXPHOS-dependent growth. These findings demonstrate that the presence of Gα$_q$ proteins at the mitochondria serves as a physiological function: stabilizing elongated mitochondria and regulating energy production in Drp1 and Opa1 dependent mechanisms. This thereby links organelle dynamics and physiology.

1. Introduction

Heterotrimeric G proteins, consisting of an α subunit and a complex formed from β and γ subunits, are well-established mediators of signal transduction pathways downstream of G protein-coupled receptors (GPCRs). For many years it was believed that G proteins perform their function at or close to the plasma membrane. Only recently did it become evident that G proteins can be localized at and signal to different endomembranes, including the endoplasmic reticulum (ER) and Golgi, and that their localization can be highly dynamic [1]. Recent findings have identified the mitochondria as a non-canonical localization for G proteins, including Gα$_{12}$ [2], Gα$_i$ [3] and Gβ2 [4]. Moreover, recent reports confirm that some G protein-effectors or binding partners, such as MAPKs, Akt, GRK2 and PKC, are also present at the mitochondria; particularly at the outer mitochondrial membrane and in the intermembrane space [5,6], which suggests that this new localization of G proteins may be functionally important.

Of the different types of Gα, the Gα$_q$ family members (including Gα$_q$, Gα$_{11}$, Gα$_{14}$ and Gα$_{15/16}$) [7] stimulate the β-isoform of phosphoinositide phospholipase C (PLC-β), which in turn increases inositol lipid (i.e., calcium/PKC) signaling [8]. The members of the human Gq family, Gα$_{11}$, Gα$_{14}$ and Gα$_{16}$, share approximately 90%, 80% and 57% homology, respectively, of their amino acid sequence with Gα$_q$ [7]. Most downstream cellular responses result from enhanced calcium signaling, but growing evidence indicates that other events may account for some of the physiological roles of Gα$_q$ family members [8]. A growing list of scaffolding/adaptor proteins (caveolin-1 [9], EBP50/NHERF1 [10], CD9/CD81 [11], Flotilin [12], TRP1 [13]), regulatory proteins (RGS [14,15]), GRK [16,17], effectors (RhoGEFs [18], Btk [19], PKCζ/ERK5 [20]) and activator proteins (Ric-8A [21], tubulin [22]) may help to explain some of the unexpected signaling pathways that they regulate [79]. The importance of different subcellular localizations of Gα$_q$ responses is still a matter of study.

* Corresponding author at: Molecular Biology Institute of Barcelona (IBMB), Spanish National Research Council (CSIC), Barcelona 08028, Spain. Tel.: +34 93 4020193.
E-mail address: aarbmc@ibmb.csic.es (A.M. Aragay).
[1] Present address: Department of Neuroimmunology, Hospital Clínic (IDIBAPS), Barcelona, Spain.

Mitochondria are essential organelles enveloped by two close but opposed membranes. The outer membrane mediates exchange between the cytosol and intermembrane space, while the inner membrane delimits the matrix space and contains respiratory complexes for oxidative phosphorylation (OXPHOS) [23]. Mitochondria can be highly dynamic organelles that fuse and divide in response to environmental stimuli, developmental status, and the energy requirements of the cell [24–26]. These events are regulated by specific proteins involved in fission and fusion, and also in the maintenance of mitochondrial distribution [27,28]. The most notable proteins involved in mitochondrial fission/fusion processes are: the dynamin-like protein DLP1/Drp1; the small helix-rich proteins Fis1 and Mff, linked to outer mitochondrial membrane fission. The dynamin-related GTPases, mitofusins (Mfn1/2), and optic atrophy 1 (OPA1), associated with the outer and inner membrane, respectively, mediate fusion of the membranes [28–33].

The presence of signaling molecules at the mitochondria highlights the possibility of novel signaling pathways that control energy production. In the search for mitochondrial localized heterotrimeric G proteins, proteomic analysis together with fractionation and immuno-fluorescence analysis show that $G\alpha_q$ and $G\alpha_{11}$ target mitochondria through their N-terminal sequence. Herein, we demonstrate that $G\alpha_q$ proteins are necessary for the maintenance of the proper balance between mitochondrial fusion and fission processes, and consequently for regulating the respiratory capacity of mitochondria.

2. Materials and methods

2.1. Materials

pcDNA3-$G\alpha_q$ and pcDNA3-$G\alpha_q$-R183C were as described elsewhere [34]. pcDNAI-$G\alpha_q$-GFP was generously provided by C. Berlot (Yale University School of Medicine, USA). $G\alpha_q$-N-terminus (1–124 aas) in pEGFP was cloned from pcDNAI-$G\alpha_q$-GFP, and $G\alpha_q$-N-terminus-FLAG in pcDNA3 was amplified by PCR. The $G\alpha_q$-N-I25/26E mutant in pEGFP was amplified by PCR using pcDNA3-$G\alpha_q$-I25/26E [34] as a template. Mt-DsRed and mt-GFP were cloned from pWPXL-mt-DsRed [35] and pWPXL-mt-GFP [35], respectively. The ER marker was obtained from Clontech (USA). pcDNA3-$G\beta_1$-FLAG, $G\beta_2$-FLAG, $G\beta_4$-FLAG and $G\gamma_2$-HA were obtained from Missouri S&T cDNA Resource (USA). HA-tagged Drp1 and Drp1-K38A in pcDNA3 were kindly provided by A. van der Bliek (University of California, LA, USA). PA-mitoGFP [36] and Plasmid 23348 were purchased from Addgene (USA). The antibodies used were: $G\alpha_q$, $G\alpha_{q/11}$, Gβ and TOM20 (Santa Cruz Biotechnology); $G\alpha_q$ internal, Porin-VDAC and Porin 31 HL (Calbiochem); SERCA2, Golgi [58K-9], GAPDH, Pan-cadherin, Mitofusin-1, Mitofusin-2 and LAMP1 (Abcam); Smac/diablo, Rab11, Drp1, COXI and OPA1 (BD Biosciences); Caveolin-1 (Zymed); complex II (anti-αFp70 kDa subunit) (Invitrogen); Hsp70 (BioReagents); FIS1 (BioVision); HA-tag (Roche); M2-Flag (Sigma Aldrich); complex I (anti-NDUFA9), complex III (anti-Core1) and complex V (anti-βATPase) (MitoSciences); and complex IV (anti-NDUFA4) (BioWorld Technology). $G\alpha_q$ transgenic mice which over-expresses mouse $G\alpha_q$ exclusively in the myocardium were a generous gift from G. W. Dorn II, Washington University at St Louis [37].

2.2. Cell culture, lysis and immunoprecipitation

NIH3T3 cells were obtained from the American Type Culture Collection (ATCC) (Manassas, VA, USA). Human embryonic kidney cells (HEK293T) were from Invitrogen (Carlsbad, CA, USA). WT, and knockout $G\alpha_{q/11}^{-/-}$ and $G\alpha_{12/13}^{-/-}$ MEFs were provided by S. Offermanns, (University of Heidelberg, Germany). WT and knock-out Mfn1$^{-/-}$ and Mfn2$^{-/-}$ MEFs were a gift from D.C. Chan (Division of Biology, California Institute of Technology, UA). HeLa cells stably expressing mt-DsRed are described elsewhere [35]. All cell types were grown in Dulbecco's modified Eagle's medium (DMEM) (Sigma, St. Louis, MO, USA), supplemented with 10% fetal bovine serum (FBS) (Invitrogen, GIBCO, USA). Cells were transiently transfected either with Metafectene Pro (Biontex, USA) or Fugene 6 (Roche, Switzerland) according to the manufacturer's instructions.

Cells were washed twice with ice-cold PBS prior to lysis in 700 μl of RIPA buffer A (0.3 M NaCl, 0.1% SDS, 50 mM Tris, pH 7.4, 0.5% deoxycholate, 1 mM Na_3VO_4, 10 mM NaF, 30 mM sodium pyrophosphate, 10 mM $MgCl_2$, 1% n-dodecyl β-D-maltoside, leupeptin 5 μg/ml, aprotinin 2 μg/ml, 1 mM PMSF) for 1 h at 4 °C. Extracts were cleared by centrifugation at 13,000 rpm for 15 min at 4 °C and the protein concentration was determined by Bradford analysis. For OPA1 immunoprecipitation, an anti-OPA1 antibody was incubated at 4 °C overnight. Protein G-sepharose was added and incubated for 1 h, and then washed several times with RIPA buffer B (buffer A with 0.01% n-dodecyl β-D-maltoside and without protease inhibitors). The samples were resuspended in Laemmli buffer. Cells were visualized with either chemiluminescence (by film acquisition or LAS3000) or infrared detection (Odyssey System). Quantifications were performed with the software indicated in the figure legends.

2.3. Imaging

For immunofluorescence, cells seeded on coverslips were washed in PBS, fixed (4% formaldehyde) and permeabilized in PBS with 0.1% Triton X-100 and 0.05% sodium deoxycholate, before staining with primary antibodies and secondary Alexa Fluor antibodies (Invitrogen, CA, USA) in blocking solution (5% goat serum). Mitochondrial morphology was determined as described elsewhere [38] and examined using a Nikon E600 microscope. Optical sections were acquired using a Leica TCS SP5 confocal system. Colocalization analyses were performed using LAS AF software (Leica Microsystems, Germany), Imaris colocalization module (Bitplane AG, Zurich, Switzerland) or ImageJ (National Institutes of Health, USA). Average mitochondrial area and length were quantified using the LAS AF software (Leica Microsystems, Germany). Scale bars of 10 μm and Z-stacks of 0.5 μm are shown (unless specified differently in the figure legends). For live imaging, cells were seeded on coverslips and transiently transfected as described above. For short-term live cell imaging, an UltraView ERS spinning disk confocal microscope (Perkin Elmer, USA) equipped with a 37 °C incubation chamber with 5% CO2 was used. Z-stacks of the images were collected using a 100× NA 1.4 oil objective with a helium-neon laser at 543 nm. The Z-stacks were acquired continuously over 10 min in the spinning disk with 300 millisecond exposures. The images from the time-lapse imaging were processed using Volocity 3D image analysis software (Perkin Elmer, USA) and mounted as MPEG4 files. For the electron microscopy, MEFs were plated in two 10 cm Ø plates for each sample and sent to the Electron Microscopy Platform (Scientific and Technological Centers, University of Barcelona, Spain) for sample preparation. Ultrathin sections (55 nm) were cut and mounted with 200 mesh cupper grid with supported film. Image acquisition was performed with a transmission electron microscope (JEOL-1010) coupled to Bioscan software (Gatan, UK).

2.4. Isolation of mitochondria

The mitochondrial isolation kit MITOISO2 (Sigma Aldrich) was utilized according to the manufacturer's instructions. The final mitochondrial pellet was layered onto a Percoll density gradient (Sigma Aldrich), and resuspended as indicated by the manufacturer. Crude mitochondrial isolation was performed as described elsewhere [39]. For trypsin/triton digestion of crude mitochondria, 200–800 μg/ml of trypsin was added to tube T (200/+, 400/++ and 800/+++) and to tube TT, 200 μg/ml of trypsin with 2% of triton X-100 was added. All the samples were incubated at 37 °C, and after 15 min, 10% FBS was added to halt digestion. The samples were centrifuged at 13,000 ×g for 2 min and washed twice with incubation buffer before adding the SDS-loading buffer and

analyzing by Western blot. Crude mitochondrial fraction from mouse heart was performed with ProteoExtract Cytosol/Mitochondria Kit (Calbiochem), following the manufacturer's instructions. Subfractions of mouse liver mitochondria were generated as described elsewhere [40].

2.5. Cellular treatments

To label mitochondria, cells were incubated with 300 nM MitoTracker® CMXRos (Invitrogen) or were transfected with pcDNA3-mt-DsRed or pcDNA3-mt-GFP. The incubation of WT and $G\alpha_{q/11}^{-/-}$ MEFs with carbonyl cyanide m-chlorophenylhydrazone (CCCP) (Sigma Aldrich) (10 µM) took place in supplemented DMEM at 37 °C for 6 and 3 h, respectively.

2.6. Down-regulation of murine $G\alpha_{q/11}$ proteins

shRNA-mediated knockdown of $G\alpha_{q/11}$ was performed using specific Mission shRNA and nontargeting Mission shRNA negative control (Sigma Aldrich). Lentivirus particle production was developed following the manufacturer's instructions in HEK293T cells and down-regulation was monitored by immunoblot analysis of cell lysates generated after 3 days of puromycin selection of infected cells.

2.7. Mass spectrometry analysis

Following mitochondrial Percoll gradient fractionation of NIH3T3 cells and SDS-PAGE, the gel was stained with Colloidal Coomassie Blue G250 (Sigma Aldrich) and the bands corresponding to 35–50 kDa were cut and sent to the PCB Proteomics Platform to proceed with mass spectrometry analysis. The related protocols can be found at http://www.pcb.ub.edu/homePCB/live/en/p1249.asp.

2.8. Mitochondrial fusion analysis

MEFs were transfected with mt-DsRed and mito-PAGFP. A cell was photobleached and photoactivated and then time lapse series of image stacks composed of 4 images (512 × 512) were taken every 4 s for 15 min. Intensity correlation analysis was performed against red (photobleached mt-DsRed) and green (photoactivated mito-PAGFP) using Volocity. The threshold was automatically performed [41]. The rates of fusion were analyzed using the overlap coefficient K2 (red dots containing green) and data were normalized according to the intensity of the first time point after photobleaching.

2.9. Growth rates

Cells (5×10^4) were plated in 24-well plates in 1 ml of the indicated medium and incubated at 37 °C for up to 3 days. They were counted daily using a Neubauer chamber. The culture media used were: DMEM with 5 mM of either glucose or galactose, supplemented with 10% FBS.

2.10. Cellular ATP, oxygen consumption and membrane potential

The ATP Determination Kit (Invitrogen) was used following the manufacturer's instructions. The oxygen consumption was determined in 4×10^4 intact MEFs using a Seahorse Bioscience XF96 extracellular flux analyzer following the manufacturer's instructions and using the materials provided. Protocol: 12 min of equilibration, followed by 3 measurements of 3 min, separated by mixing for 4 min. Uncoupled mitochondrial respiration was induced by injection of 1 µM CCCP. To stop the mitochondrial-dependent oxygen consumption, we utilized 1 µM Oligomycin. To calculate the membrane potential, MEFs (5×10^6) were treated with 100 nM of the fluorescent dye TMR for 30 min at 37 °C, washed with PBS and resuspended with 400 µl of trypsin. To halt trypsin digestion, 1 ml of PBS containing 5% BSA was added. The cells

were passed through a flow cytometer, MoFlo (Beckman Coulter) at 590 nm.

2.11. Isolation of respiratory complexes and supercomplexes — BN-PAGE

Mitochondria were isolated from cultured cell lines as described elsewhere [42], with slight modifications [39]. Digitonin-solubilized mitochondrial proteins (50 µg) were separated on blue native gradient gels (3%–13% acrylamide).

2.12. Statistical analysis

Average mitochondrial surface area: Comparison between WT and knockout cells presented heterogeneous variance, so the Mann–Whitney non-parametric test was utilized. Comparisons between values found for shRNA presented normal distributions, which allowed the use of variance analysis, followed by Student's t-test. Mitochondrial length: Values from WT and knockout cells presented heterogeneous variance, so the Mann–Whitney non-parametric test was performed; a heterogeneous variance distribution was also found in the shRNA groups, for these values the Kruskal–Wallis test was utilized. Mitochondrial morphology: The values were analyzed by Chi-squared test, only when fewer than five values were found was the G-test employed, followed by Fisher's test. Mitochondrial fusion analysis by mt-PAGFP was performed using ANOVA. Mitochondrial membrane potential and O_2 consumption were analyzed by unpaired t-test; whereas total ATP content and Odyssey quantification of Supercomplex I + III + IV/Porin was by paired t-test. Growth rate differences were determined by one-way ANOVA followed by Tukey's Test (p-values are given in the figure legends).

3. Results

3.1. $G\alpha_{q/11}$ proteins localize at mitochondria

In order to search for signaling proteins located at the mitochondria, a proteomic analysis of a mitochondrial fraction, obtained from a Percoll gradient, was performed on NIH3T3 cells. Only the gel bands around the overall molecular weight of G proteins (35–56 kDa) were chosen for sample analysis. Of 56 proteins (Table S1), 49 were either mitochondrial proteins included in MitoCarta [43], or cited as putative mitochondrial-associated proteins; this validated our approach. Among them, both $G\alpha_q$ and $G\alpha_{11}$ were recognized, as were the $G\alpha_{i2-3}$ and $G\alpha_{o1}$ subunits. $G\alpha_i$ proteins had previously been reported to be located at the mitochondria [3]. MitoProt analysis of the G proteins gave the highest scores for $G\alpha_q$ and $G\alpha_{11}$ proteins: 30% and 37%, respectively (Fig. S1). Western blot analysis of the Percoll-gradient mitochondrial fraction agreed with the proteomic analysis (Fig. 1A). A band recognized by the common anti-$G\alpha_q$ and anti-$G\alpha_{11}$ antibody was present (13%) in the fraction, as was the mitochondrial protein porin (38%). In order to obtain the purest mitochondria sample, only a fraction of total porin was recovered. A crucial finding was that no plasma membrane (P-Cadherin), ER (SERCA2) or Golgi contamination was present. The fraction did, however, contain lysosomes (20%) and caveolin-1 (4%), a protein that binds to $G\alpha_q$ [44] and is also present in mitochondria [45].

The subcellular localization of $G\alpha_q$ was analyzed in a transgenic mouse line containing 40 copies of the $G\alpha_q$ gene expressed in the myocardium. Mitochondrial fractionation showed that approximately 10% of total $G\alpha_q$ is present in the mitochondrial fraction of the wild-type (WT) heart (Fig. 1B). Interestingly, the transgenic mice showed increased levels of $G\alpha_q$ (55% of total) in the mitochondrial fraction (Fig. 1B). Again, these data indicate the presence of $G\alpha_q$ at the mitochondria in heart tissue of wild type animals and increase amounts in the transgenic mouse line. Interestingly, these mice present dilated cardiomyopathy [37] which has been reported to be associated with increased mitochondrial ROS production [46].
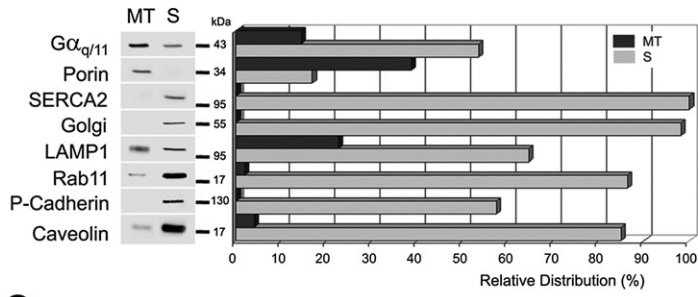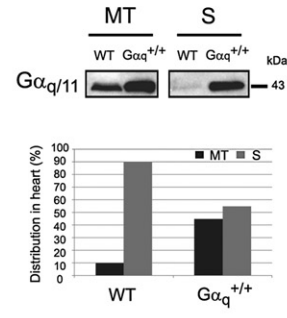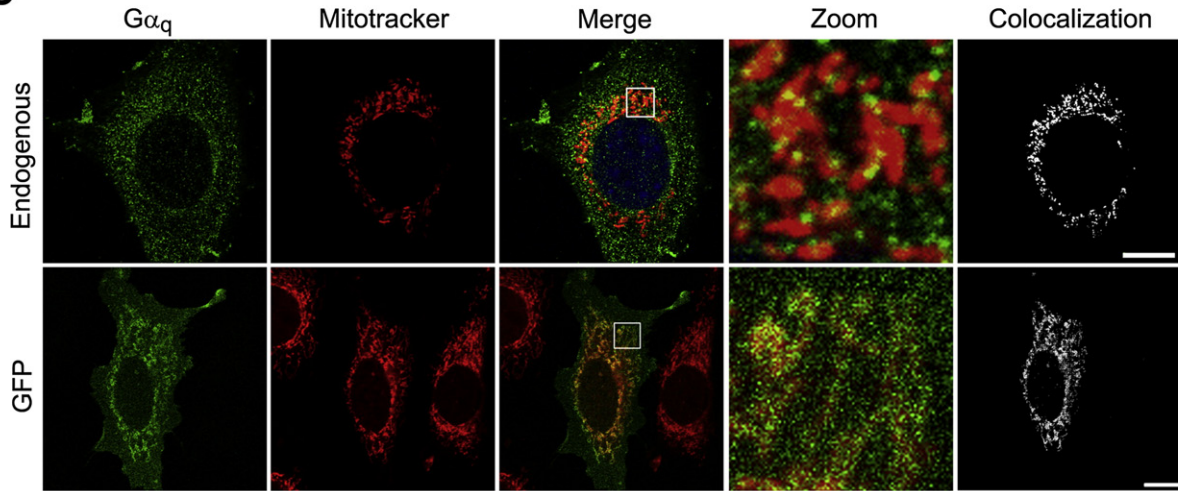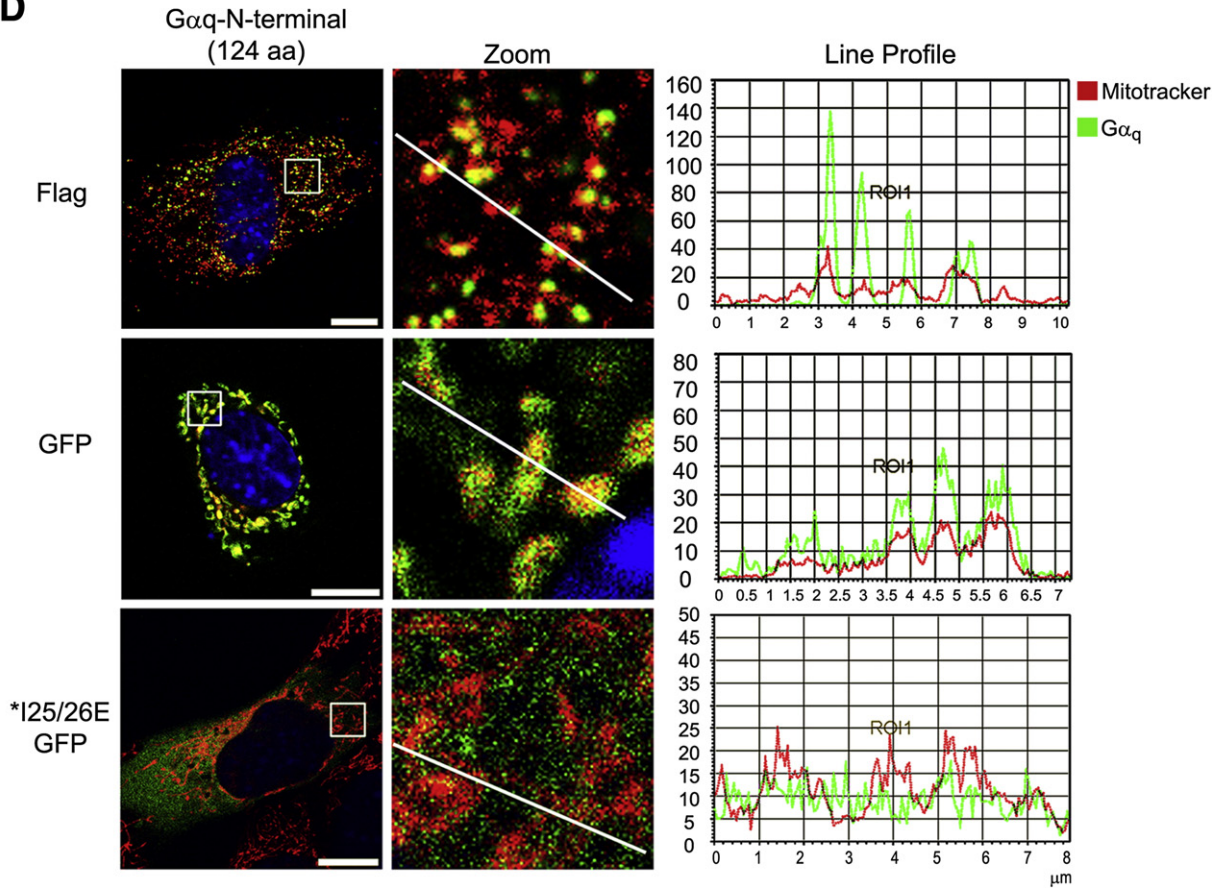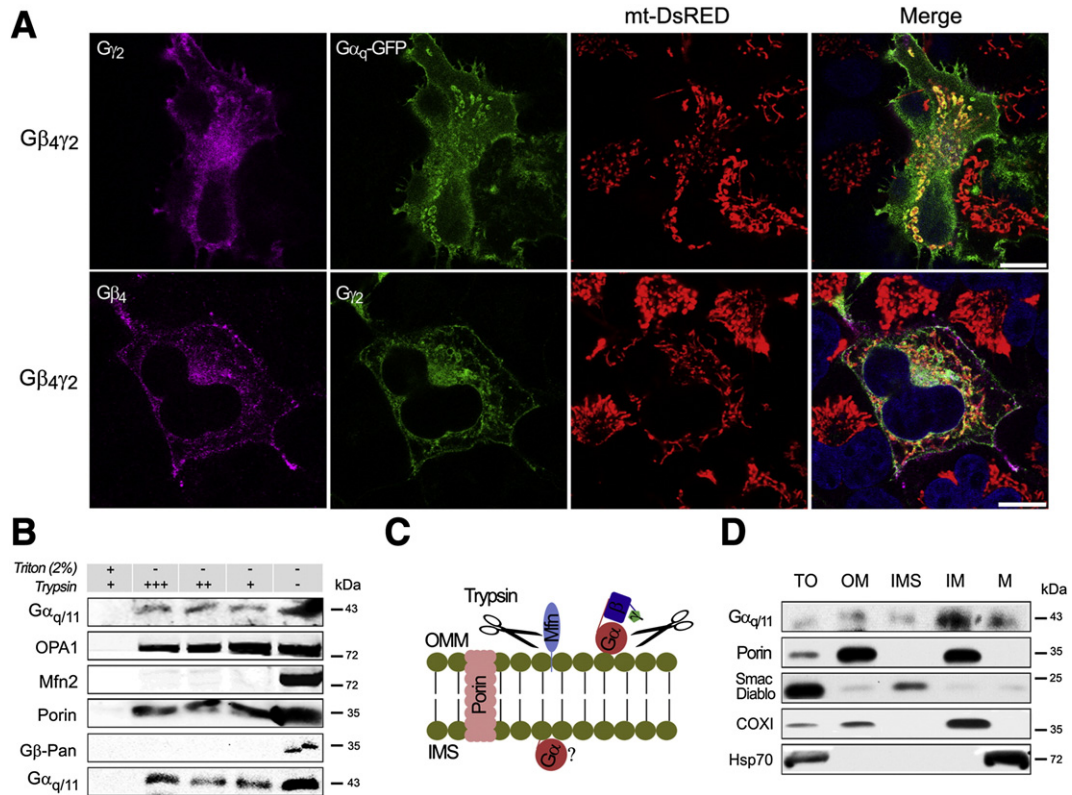
Fig. 2. $G\alpha_q$ and different $G\beta\gamma$ dimers localized at the mitochondria. (A) Confocal micrographs of HeLa cells stably expressing mt-DsRed and Gβ4-Flag γ2-HA and/or $G\alpha_q$, immunostained with anti-Flag or HA and mounted with DAPI. (B) Mitochondrial fractions of NIH3T3 cells submitted to trypsin digestion in the presence or absence of Triton X-100, immunoblotted with anti-$G\alpha_{q/11}$, OPA1 (inner membrane), Mfn2 (outer membrane), Porin (integral outer membrane) and Gβ-Pan (representing Gβγ dimer). (C) Diagram showing the likely actions of trypsin on proteins blotted in B. (D) Mouse liver mitochondrial sub-fractions shown the presence of $G\alpha_{q/11}$ at the inner membrane, immunoblotted with $G\alpha_{q/11}$ and markers: Porin (OM), Smac/Diablo (IMS), COXI (IM) and Hsp70 (M).

On the other hand, immunofluorescence analysis of the endogenous proteins in NIH3T3 cells with anti-$G\alpha_{q/11}$ antibodies (Fig. 1C) revealed a punctuated cytoplasmic pattern coincident with the mitochondria. Expression of a functional $G\alpha_q$-GFP also showed considerable localization at the mitochondria in NIH3T3 (Fig. 1C). Taken together, these findings support the hypothesis that $G\alpha_q$ proteins are located at the mitochondria.

3.2. The N-terminal region of $G\alpha_q$ is necessary for mitochondrial targeting

Considering the possibility that $G\alpha_q$ and/or $G\alpha_{11}$ were targeted to mitochondrial membranes, we searched for putative targeting sequences. A mitochondrial target prediction by Mitoprot analysis of different G alpha subunit sequences showed that mouse $G\alpha_q$ and $G\alpha_{11}$ had 30 and 37% probability of being target to mitochondria, respectively, whereas $G\alpha_{12}$, $G\alpha_{i1-2}$ or $G\alpha_o$ had lower probabilities (Fig. S1). Chimeric proteins were designed that contained the first 124 N-terminus amino acids or the C-terminus sequence of $G\alpha_q$ fused to either GFP or Flag. The C-terminus sequence fused to GFP gave almost no detectable expression around any part of the cell. The $G\alpha_q$-protein N-terminus sequence flagged with either Flag or GFP showed mitochondrial localization (Fig. 1D), which suggests that the N-terminus of $G\alpha_q$ is sufficient for the protein to be located at the mitochondria. The $G\alpha_q$ N-terminus region contains both the

S-palmitoyl cysteines (9–10 aa) required for plasma membrane binding, and also the contact sites for Gβγ interaction. Mutations of amino acids 25 and 26 (IE>AA) are reported to alter Gβγ binding and also to prevent correct palmitoylation of the Gα subunit [47]. The N-terminus-$G\alpha_q$-IE25/26AA mutant (Fig. 1D) failed to localize at the mitochondria, suggesting that the interaction with Gβγ and/or the state of palmitoylation of the protein is important for mitochondrial targeting. The fact that the mutated peptide was not present at the mitochondria rules out possible artifactual localization of the chimeric protein at the mitochondria.

3.3. The $G\alpha_q\beta\gamma$ heterotrimer is localized at the outer membrane and the $G\alpha_q$ subunit at the inner membrane

The previous results suggest that the Gβγ dimer could help to target the heterotrimer at the mitochondria. The expression of Gβ4γ2 alone or together with the $G\alpha_q$-GFP protein shows the localization of both HA-tagged Gγ2 and $G\alpha_q$ with mt-DsRed (Fig. 2A and Movies S1 and S2). Similar results were obtained by expressing Gβ1γ2 together with $G\alpha_q$-GFP (Fig. S2A). The Gβγ subunits are known to localize at the ER of cells [1]. To establish whether Gβγ localization corresponded to the ER, we compared the localization of Gβ4γ2 in HeLa cells expressing

Fig. 1. $G\alpha_q$ and $G\alpha_{11}$ are localized at the mitochondria. (A) Distribution of endogenous $G\alpha_{q/11}$ and organelle markers in the mitochondrial (MT) and supernatant (S) fractions obtained by Percoll gradient of NIH3T3 cells. The MT fraction was resuspended in 1/5 of initial volume, and equal volumes of MT and S fractions were loaded in the gel and immunoblotted with: anti-$G\alpha_{q/11}$, Porin (mitochondria), SERCA2 (ER), Golgi, LAMP1 (lysosomes), Rab11 (ribosomes), P-cadherin (PM) and Caveolin-1 as a protein that binds to $G\alpha_q$ [44] and is present at the mitochondria [45]. Quantification was performed by Multi-Gauge. (B) $G\alpha_q$ heart-specific transgenic mouse ($G\alpha_q^{+/+}$) shows increased amount of $G\alpha_q$ at the mitochondria. The mitochondrial (MT) and supernatant fraction (S) was immunoblotted with $G\alpha_{q/11}$ antibody. Quantification was performed by Alpha Ease FC. (C) Confocal micrographs of NIH3T3 cells (endogenous) immunostained with anti-$G\alpha_{q/11}$ or expressing $G\alpha_q$-GFP. Colocalization was performed by LAS AF. (D) Confocal micrographs of NIH3T3 cells incubated with MitoTracker® (red) and transfected with $G\alpha_q$-N-terminus (1–124 aa) GFP and Flag, immunostained with anti-Flag and mounted with DAPI. MEF cells transiently expressing $G\alpha_q$ IE25/26AA mutants incubated with MitoTracker® (red), immunostained with anti-$G\alpha_{q/11}$ and mounted with DAPI. Line profile was generated by LAS AF.

mt-DsRed and ER-DsRed. Significantly more Gβ4γ2 was observed at the mitochondria than at the ER (Fig. S2B). These results confirm the localization of the heterotrimer at the mitochondria.

To examine the location of the G proteins within the mitochondrial subcompartments, we carried out trypsin digestion experiments on isolated mitochondria. Incubation of mitochondria with trypsin leads to the complete digestion of the outer membrane protein Mfn2 as well as that of the Gβ proteins (Fig. 2B), which is indicative of their outer membrane localization. The $G\alpha_{q/11}$ proteins were partially digested by trypsin, indicating that some protein was located together with Gβγ at the outer membrane. However, a considerable amount of $G\alpha_{q/11}$ was protected from digestion, as also observed for the inner membrane protein OPA1 (see Fig. 2C for a diagram representing trypsin digestion). Sub-fractionation of mitochondrial membrane by established procedures [40,48] yields fractions enriched in outer membrane (OM), intermembrane space (IMS), inner membrane (IM) and matrix (M). In adult mouse liver (Fig. 2D), we observed the presence of $G\alpha_{q/11}$ in the total mitochondrial fraction (TO) and associated with OM, and a relative enrichment in the IM fraction (also COXI enriched); this confirms the trypsin experimental results.

Taken together these results corroborate the presence of $G\alpha_{q/11}$ proteins in the mitochondria of different cells and tissues, and also suggest that those proteins are localized together with Gβγ at the outer membrane. A proportion of the $G\alpha_{q/11}$ subunits are protected from digestion, suggesting that they are localized inside the mitochondria.

3.4. $G\alpha_{q/11}$ deletion results in defects in mitochondrial morphology

As a first approach to determine whether $G\alpha_{q/11}$ plays a direct functional role when localized at the mitochondria, we compared mitochondria from $G\alpha_{q/11}^{-/-}$ knockout (KO) and wild type murine embryonic fibroblasts (MEFs). Confocal microscopy of cells expressing the mitochondrial target peptide mt-DsRed showed marked differences in mitochondrial distribution and shape (Fig. 3A). Notably, mitochondria from $G\alpha_{q/11}^{-/-}$ cells were compacted around the nucleus. These differences were also observed via in vivo time-lapse images of WT (Movie S3) and $G\alpha_{q/11}^{-/-}$ (Movie S4) MEFs. Quantification of average mitochondrial surface area (Fig. 3B) showed that in $G\alpha_{q/11}^{-/-}$ cells, the mitochondrial network is less distributed throughout the cell. Quantification of the mitochondrial length showed that the $G\alpha_{q/11}^{-/-}$ mitochondria were also more fragmented than those in WT cells (Fig. 3C). These results were corroborated using WT MEFs treated with shRNA against $G\alpha_q$ (Fig. S3A). The $G\alpha_q$-down-regulated cells showed an increased compaction of their mitochondrial network and more fragmented mitochondria (Fig. 3D–F) relative to the scrambled shRNA. When $G\alpha_q$ and $G\alpha_q$-GFP
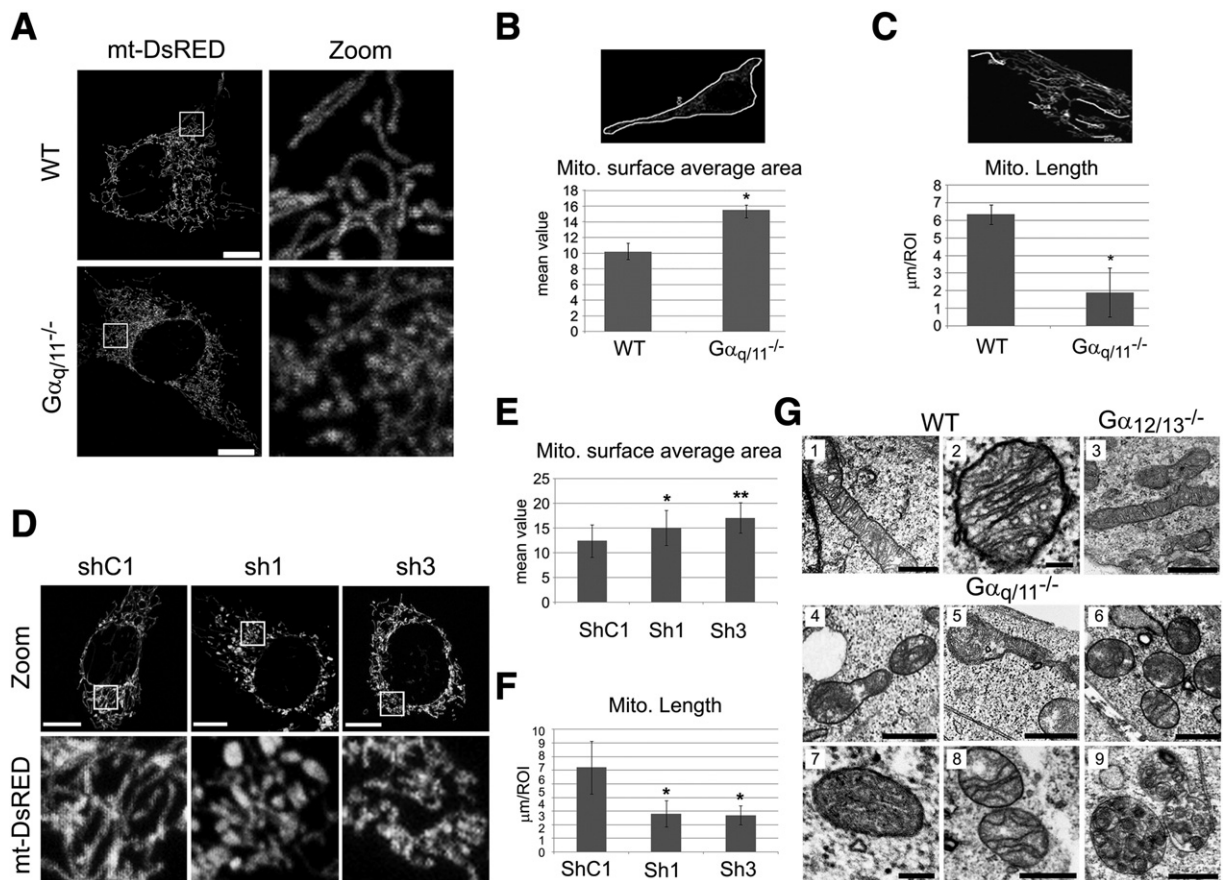
Fig. 3. MEF $G\alpha_{q/11}$ knockout ($G\alpha_{q/11}^{-/-}$) and shRNA depleted cells show alterations of the mitochondrial network and morphology. (A) Representative confocal micrographs of MEF wild-type (WT) and $G\alpha_{q/11}^{-/-}$ cells expressing the mitochondrial matrix-targeted mt-DsRed after 24 h of transfection. (B) Mitochondrial surface average area calculated by the Polygon ROI with LAS AF software. The mean value of different intensities inside the ROI is related to the distribution of the fluorochrome. Data represent mean ± s.d. (n = 45). Mann–Whitney test was employed (*p < 0.0001). Experiments were carried out as in A. (C) Mitochondrial length was calculated by the polyline measurement. Data represent mean ± s.d. (n = 25) for 10 ROIs each. Mann–Whitney test was utilized (*p < 0.0001). Experiments were carried out as in A. (D) Representative confocal micrographs of MEF wild-type cells infected by a lentivirus containing two different sequences of shRNA (1 and 3) against $G\alpha_{q/11}$ and one control shRNA (shC1) expressing mt-DsRed protein after 24 h of transfection. (E) Experiments were carried out as in D and calculated as in B. Data represent mean ± s.d. (n = 25). Student's t-test was employed (*p = 0.0063 and **p < 0.001). (F) Experiments were carried out as in D and calculated as in C. Data represent mean ± s.d. (n = 25). Kruskal–Wallis test was utilized (*p < 0.0001). (G) TEM micrographs showing the mitochondrial ultrastructure of MEFs WT (1–2), $G\alpha_{q/11}^{-/-}$ (4–9) and $G\alpha_{12/13}^{-/-}$ (3) cells. Scale bars: 0.5 μm and 0.1 μm in 2. See also Fig. S3C for more micrographs of $G\alpha_{12/13}^{-/-}$ cells.

(Fig. S3B) were re-expressed in the $G\alpha_{q/11}^{-/-}$ MEF cells, both proteins restored the normal mitochondrial morphology and resulted in a fused mitochondrial network. The $G\alpha_q$ N-terminus (the first 124 aas) did not achieve this (Fig. S3B), demonstrating that the whole protein is required for the recovery of the mitochondrial phenotype.

To corroborate the immunofluorescence results, the ultrastructure of the $G\alpha_{q/11}^{-/-}$ mitochondria was examined by transmission electron microscopy (TEM). The TEM images revealed mitochondrial abnormalities (Fig. 3G, 4–9) compared with WT (Fig. 3G1 and G2) or $G\alpha_{12/13}^{-/-}$ mitochondria (Figs. 3G3 and S3C). The $G\alpha_{q/11}^{-/-}$ mitochondria showed localized swelling accompanied by a constriction along the length of the mitochondria (Fig. 3G4 and G5). Almost no elongated mitochondria were found, thereby corroborating the immunofluorescence results. Remarkably, some mitochondria seem to be devoid of a cristae structure (Fig. 3G5–7) and the openings of cristae junctions appeared very narrow (Fig. 3G8). We also observed an increased number of autophagosomes containing mitochondrial remnants (Fig. 3G9), suggesting a greater turnover of damaged mitochondria through the process called mitophagy. Overall, these results suggest that $G\alpha_{q/11}$ proteins play an essential role in mitochondrial morphology.

3.5. $G\alpha_q$-GDP state is needed to coordinate elongation of the mitochondrial network

The aforementioned changes in mitochondrial morphology associated with alterations in $G\alpha_q$ expression could be the result of alterations in the processes of fission or fusion. To determine whether $G\alpha_{q/11}$ is involved in mitochondrial fusion, we transfected a photoactivated mito-PAGFP into WT (Movie S5) and $G\alpha_{q/11}^{-/-}$ (Movie S6) MEFs. A constant increase in mitochondrial fusion events over time was detected in both cell types, but the rate of mitochondrial fusion in the $G\alpha_{q/11}^{-/-}$ cells was significantly lower than that in WT MEFs (Fig. 4A). These results suggest that a lack of $G\alpha_{q/11}$ affects mitochondrial fusion events over time.

To study the effect of $G\alpha_q$ on fusion events further, we expressed $G\alpha_q$ in Mfn2$^{-/-}$ and Mfn1$^{-/-}$ depleted MEFs. It is well documented that Mfn1 and Mfn2 are involved in mitochondrial fusion and, in their absence, mitochondria present a fragmented phenotype (Fig. 4B) [49]. $G\alpha_q$ expression in these cells induced a significant increase in the elongation of the Mfn2$^{-/-}$ mitochondria (Fig. 4C), which indicates that $G\alpha_q$ expression promotes fusion. As expected, $G\alpha_q$ was unable to induce elongation in Mfn1$^{-/-}$ cells, since the protein is essential for mitochondrial fusion, which corroborates previous findings [49]. The activated form of $G\alpha_q$, $G\alpha_q$-R183C, did not produce the same effect (Fig. S4A). These results suggest that a GDP state of $G\alpha_q$ is needed for this function.

In contrast, expression of $G\beta2\gamma2$ in Mfn2$^{-/-}$ cells promoted mitochondrial bundle-like aggregation and perinuclear clustering (Fig. 4D) similar to those seen following mitofusin overexpression [50]. However, when $G\alpha_q$ was expressed alone or together with the heterodimer, a hyperfused-mitochondrial network was observed in both WT and Mfn2$^{-/-}$ cells (Fig. 4D). The fact that $G\beta\gamma$ did not phenocopy the effect of $G\alpha_q$ suggests that these subunits play complementary roles at the mitochondria; this provides further evidence that $G\alpha_{q/11}$ regulates fusion and/or fission events at the mitochondria.
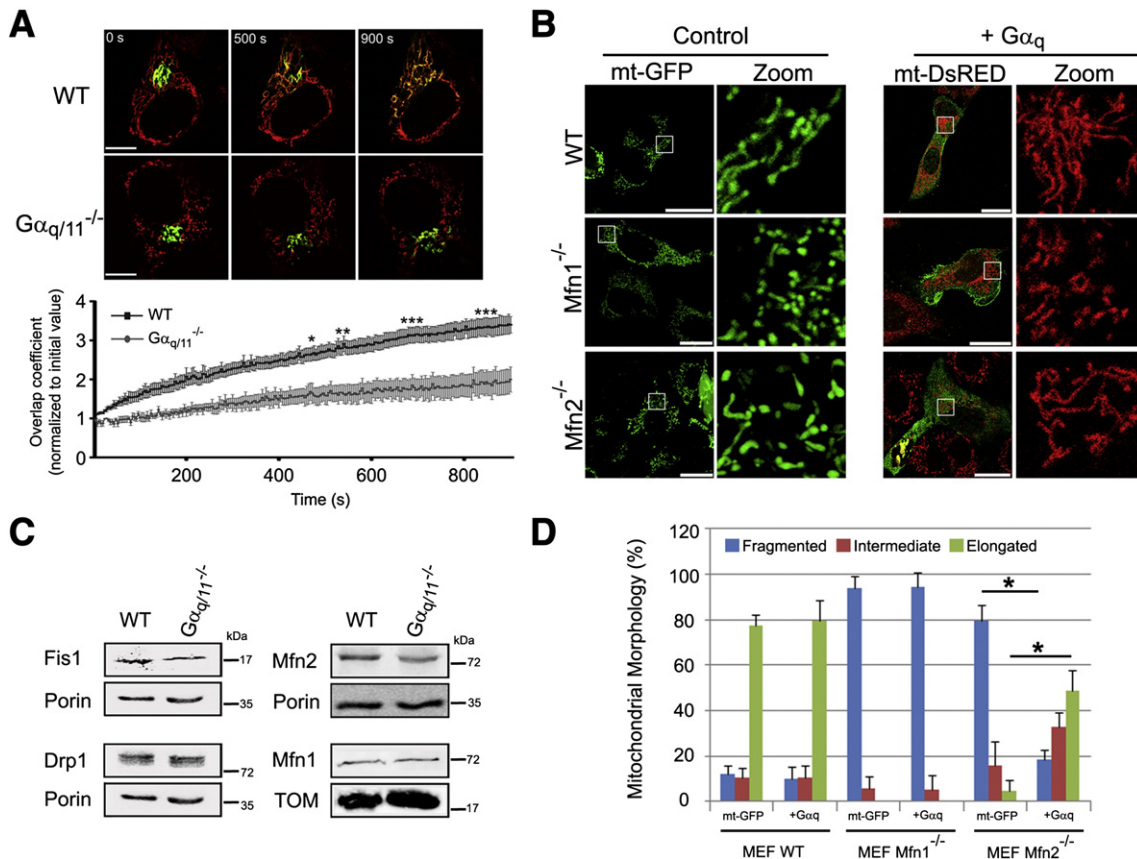
Fig. 4. Impairment in mitochondrial fusion in the absence of $G\alpha_{q/11}$. (A) MEFs transfected with mt-DsRed and mito-PAGFP. Mito-PAGFP was photoactivated, mt-DsRed was photobleached at t = 0 s. Panels show the same cell at a range of time points. Scale bar: 75 μm. Data show mean ± s.e.m (n = 5). ANOVA (*p < 0.05, **p < 0.01 and ***p < 0.001) was employed. (B) Confocal micrographs of MEFs transfected with mt-GFP or $G\alpha_q$/mt-DsRED, immunostained with anti-$G\alpha_{q/11}$ antibody (right panel in green). Zoom shows only mitochondria. Scale bar: 25 μm. (C) Mitochondrial morphology was scored from B. Data represent mean ± s.d. (n = 50) of three independent experiments. Chi-Square test was employed (*p < 0.0001). (D) Confocal micrographs of MEFs in the presence of $G\beta2$-Flag (green on left and purple on right panel)/mt-dsRED with or without $G\alpha_q$-GFP (green on right panel) mounted with DAPI (blue). Zoom shows only mitochondria.
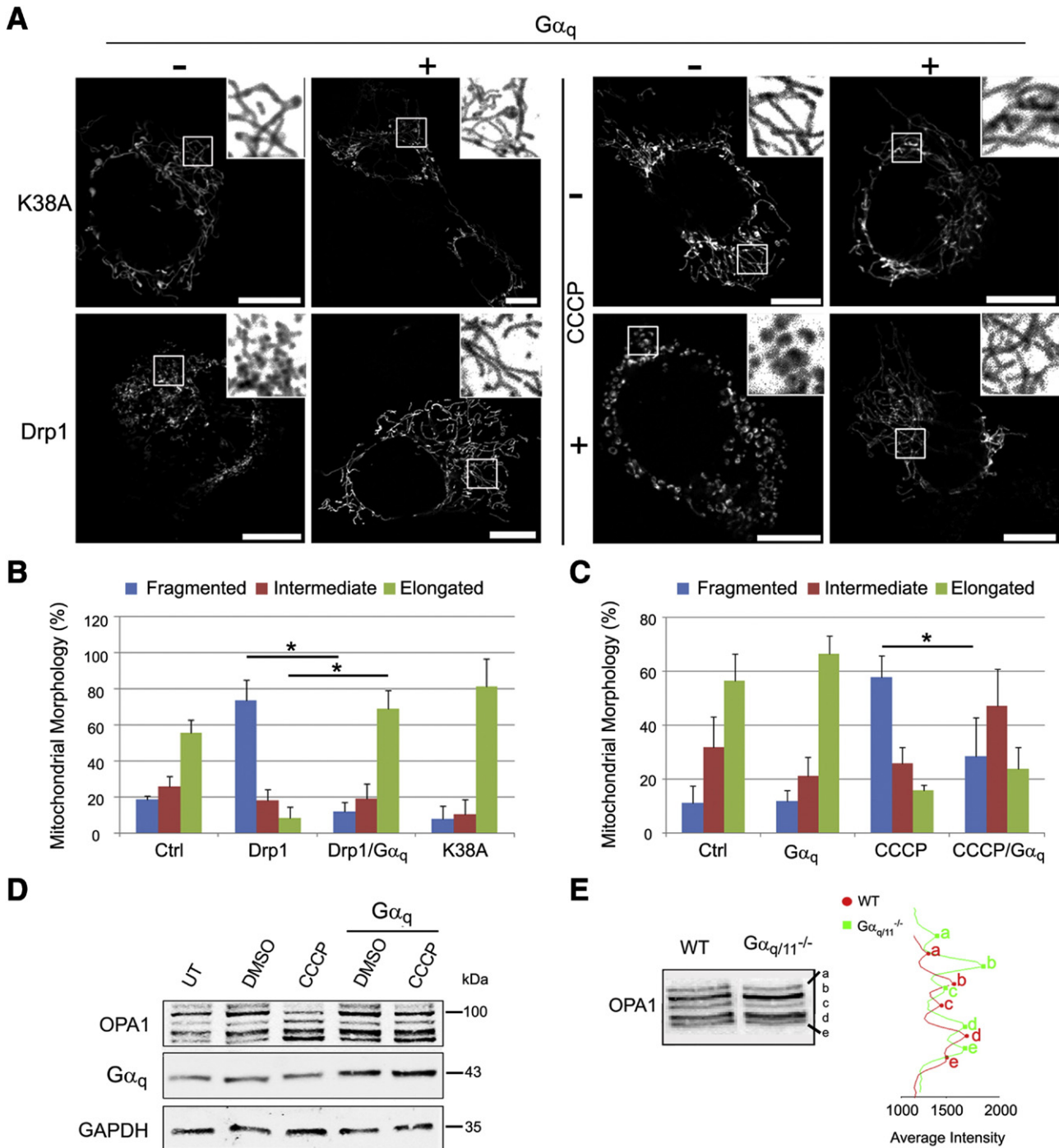
Fig. 5. $G\alpha_q$ stabilizes mitochondrial fusion, blocking fragmentation induced by Drp1 or CCCP. (A) Confocal micrographs of MEF wild-type cells transfected with mt-DsRed (gray) and Drp1-HA or Drp1-(K38A)-HA or treated with 10 µM CCCP (+) or DMSO (−) for 3 h, overexpressing (+) or not (−) $G\alpha_q$, immunostained with anti-HA and anti-$G\alpha_{q/11}$ (not shown). (B–C) Mitochondrial morphology quantified as mentioned in Fig. 4C. Chi-Square test was employed (*p < 0.0001). Experiments were carried out as in A. Data represent mean ± s.d. (n = 50) of three independent experiments. (D) MEF cells were transfected with pcDNA3 or pcDNA3-$G\alpha_q$ and the day after being incubated for 3 h with 10 µM CCCP or DMSO. Lysates were immunoblotted with the indicated antibodies. (E) MEF WT and $G\alpha_{q/11}^{−/−}$ cells immunoprecipitated for OPA1 isoforms and immunoblotted with OPA1 antibody, quantified by Line Profile of Odyssey System.

3.6. $G\alpha_q$ stabilizes mitochondrial fusion, blocking fragmentation induced by Drp1 expression

Expression in cells of the dynamin-like protein, Drp1, induces strong mitochondrial fragmentation (fission) in contrast to the expression of its mutant form Drp1K38A (Figs. 5A and S5). We used the fragmentation capacity of Drp1 as another approach to study the effect of $G\alpha_q$ on mitochondrial fission. The fragmentation induced by Drp1 was significantly diminished upon $G\alpha_q$ expression in WT cells (Fig. 5B and C). Mitochondrial elongation was also augmented in $G\alpha_{q/11}^{−/−}$ cells expressing Drp1K38A, which recovered the fragmented phenotype (Fig. S5). $G\alpha_q$ acts as a potent inhibitor of mitochondrial fission, with its action depending on Drp1 at the mitochondria.

MEFs were treated with the uncoupling agent CCCP, which reduces mitochondrial fusion through dissipation of the mitochondrial membrane potential ($\Delta\Psi$m) and OPA1 degradation. The fragmentation of

mitochondria observed in the presence of CCCP (10 μM) decreased significantly in the presence of Gα$_q$ (Figs. 5A, C and S5). Analysis of the OPA1 isoforms shows that CCCP could induce the degradation of OPA1, decreasing the higher isoforms (bands a and b) and increasing bands d and e (Fig. 5D), as expected. Consistently with this, cells expressing Gα$_q$ present less decrease in bands b and e upon CCCP treatment. A change in the proportion of OPA1 bands was also observed in the untreated Gα$_q$ and Gα$_{11}$ knock-out cells (Fig. 5E), which presented higher levels of bands b and e. We detected no major changes in the expression of the fusion and fission proteins (Fig. S5B) that could explain these effects. The results suggest that Gα$_q$ and Gα$_{11}$ affect the proteolytic cleavage of OPA1 protein via either a direct or indirect effect, thus impinging on the mitochondrial fission and cristae structure.

3.7. A lack of Gα$_{q/11}$ proteins leads to significant decreases in ΔΨm, overall respiratory capacity, ATP production and OXPHOS dependent growth

The results suggest that Gα$_q$ and Gα$_{11}$ proteins are necessary to maintain a proper balance of fusion and fission, and also for maintaining crest morphology. At the inner mitochondrial membrane, a proton gradient that drives ATP production is created by the respiratory complexes passing electrons through the electron transport chain and giving rise to the ΔΨm. To establish whether Gα$_{q/11}$ proteins are necessary for normal mitochondrial bioenergetics, we first measured the intensity of tetramethyl rhodamine (TMR) fluorescence. We determined that the ΔΨm of Gα$_{q/11}^{-/-}$ cells was significantly lower than that of WT cells (Fig. 6A). A recovery of the Gα$_{q/11}^{-/-}$ cells through the expression of Gα$_q$ prevented this decrease in ΔΨm. In addition, we determined the endogenous ATP levels and the O$_2$ consumption rates (OCRs) in WT and Gα$_{q/11}^{-/-}$ cells (Fig. 6B and C). Cells lacking Gα$_{q/11}$ have 15% less cellular ATP (Fig. 6B) and lower OCRs both under baseline conditions and when maximum respiratory capacity is activated by mitochondrial depolarization with CCCP (Fig. 6C).

To gain a fuller understanding of the underlying nature of the mitochondrial electron transport chain alterations, we determined how the absence of Gα$_{q/11}$ alters the assembly of the respiratory complexes using BN-PAGE followed by immunoblotting for subunits of the respiratory chain (Fig. 6D–H). Gα$_{q/11}^{-/-}$ cells had reduced amounts of dimer complex V (Fig. 6D). Moreover, significantly less of the supercomplexes I + III + IV (Fig. 6I) were observed. The critical reduction in larger complexes could be related to the narrow and disrupted cristae observed by TEM (Fig. 3G). Therefore, the absence of
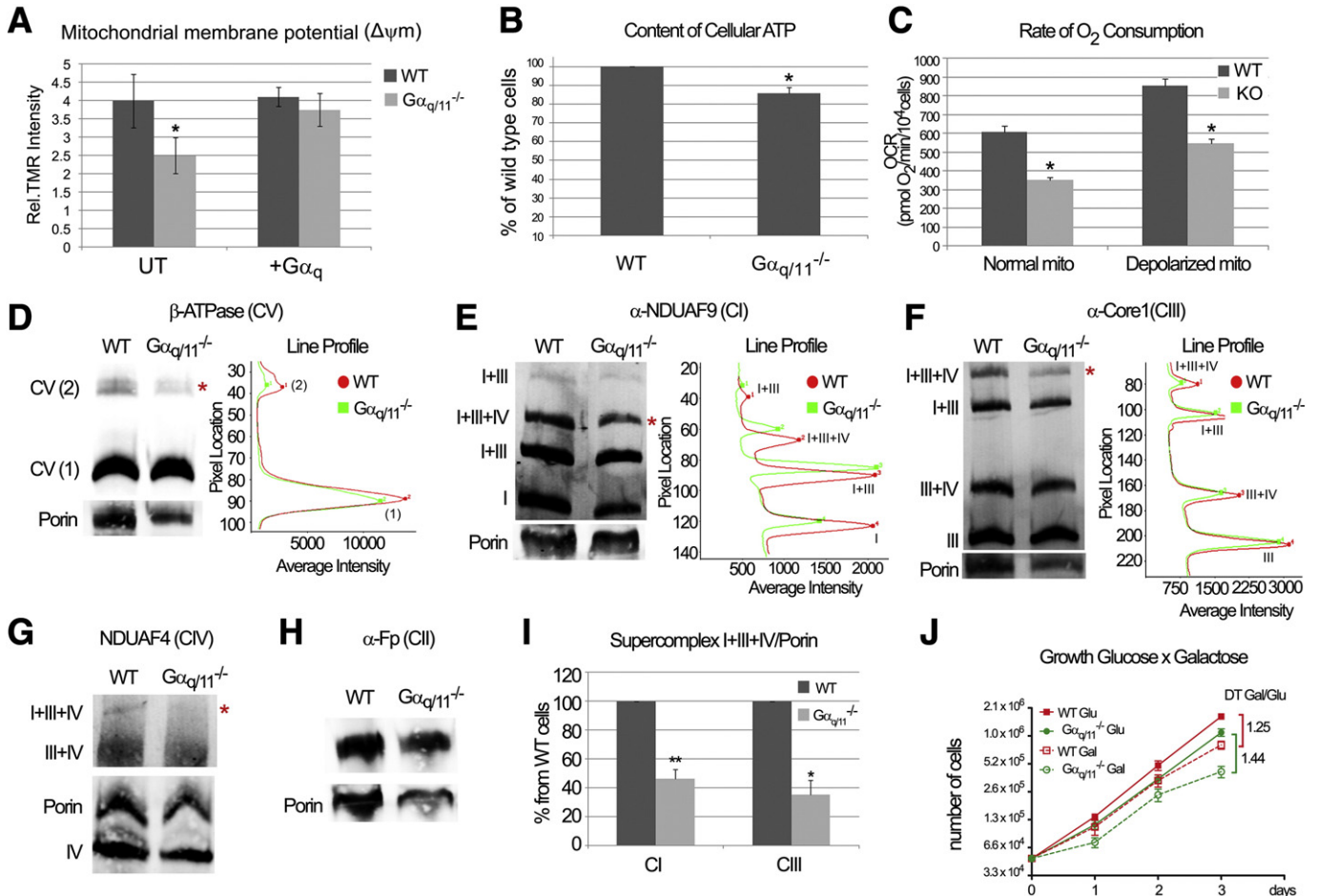
Fig. 6. Gα$_{q/11}$ is needed for normal mitochondrial function and respiratory supercomplex assembly. (A) MEF Gα$_{q/11}^{-/-}$ cells show decreased mitochondrial membrane potential (ΔΨm). +Gα$_q$ indicates that cells were transfected with pcDNA3-Gα$_q$ the day before analysis. Data represent mean ± s.d. (n = 4 WT and n = 6 KO). Unpaired t-test was employed (*p = 0.0023). (B) Decreased content of cellular ATP is observed in Gα$_{q/11}^{-/-}$ cells. Data represent mean ± s.d. (n = 4) with normalized values respect to WT (%). Paired t-test (*p = 0.0014) was utilized. (C) Gα$_{q/11}^{-/-}$ cells present less oxygen consumption (OCRs) rate. After baseline measurements (normal mito) cells were depolarized (CCCP). Data represent mean ± s.e.m (n = 18 WT and n = 20 KO). Unpaired t-test (*p < 0.0001) was employed. (D–H) Mitochondria from MEFs were lysed in digitonin and resolved by BN-PAGE then blotted to determine native complexes and supercomplexes: (D) Complex V (β-ATPase); (E) Complex I (detected by α-NDUFA9); (F) Complex III (α-Core1); (G) complex IV (NDUFA4) and (H) complex II (α-Fp). (I) Ratio of supercomplexes I + III + IV per Porin, quantified by Odyssey System utilizing experiments from E and F. Data represent mean ± s.d. (n = 5 CI and n = 3 CIII). Paired t-test (**p < 0.0001, *p < 0.01) was utilized. * denotes changes in supercomplex band intensity. (J) Cell growth in glucose (Glu) versus galactose (Gal) per days and doubling time (DT) ratio. Statistical significance was found by one-way ANOVA followed by Tukey's test after day 2 in both conditions for KO compared to WT cells (p < 0.05). Data represent mean ± s.e.m (n = 6).

$G\alpha_{q/11}$ results in assembly disorganization of the respiratory supercomplexes which alters organelle energy production.

To determine whether the observed alterations in mitochondrial OXPHOS promoted by a lack of $G\alpha_{q/11}$ were functionally relevant, we studied the growth of the cells in a medium in which glucose was substituted by galactose; conditions that render the cells highly dependent on ATP produced by OXPHOS. Thus, the doubling time (DT) of both WT and $G\alpha_{q/11}^{-/-}$ cells increases in galactose compared to that in glucose as a consequence of the adaptation to a more OXPHOS demanding medium (Fig. 6J). The increase in DT is higher in KO cells than in controls (1.44 vs. 1.25), which shows that $G\alpha_{q/11}^{-/-}$ cells have more difficulties adapting to galactose. Altogether, these results demonstrate that $G\alpha_{q/11}$ cells are required not only for proper mitochondrial dynamics but also for OXPHOS function.

4. Discussion

Our studies provide insight into the mitochondrial location and functions of the G proteins, focusing on the $G\alpha_q$ family of proteins, which are distinct from their capacity to signal through GPCRs at the plasma membrane. The results establish a previously unknown link between mitochondrial fission and fusion, energy metabolism and the $G\alpha_q$ class of G proteins. The heterotrimeric G protein ($G\alpha_{q/11}\beta\gamma$) in its basal state (GDP form) is found at the outer mitochondrial membrane; whereas the alpha subunit ($G\alpha_{q/11}$) is alone inside the organelle. At the outer mitochondrial membrane, $G\alpha_q\beta\gamma$ induces mitochondrial elongation dependent on the activity of mitofusin-1 and also reduces Drp1 induction of fission. The absence of $G\alpha_{q/11}$ affects OPA-1 isoforms, cristae structure, membrane potential and organelle bioenergetics, accompanied by a reduction in respiratory supercomplex assembly. The presence of $G\alpha_{q/11}$ proteins at the mitochondria serves as a new non-canonical pathway that stabilizes elongated mitochondria and regulates energy production, thereby linking organelle dynamics and physiology.

The role and location of G proteins at the mitochondria have not previously been explored in detail, despite the presence of these proteins in other endomembranes [51–56]. Nevertheless, there are recent reports of $G\alpha_i$, $G\alpha_{12}$ and $G\beta_2$ localization at mitochondria [2–4]. Adding to what has already been reported, $G\alpha_{o1}$, $G\alpha_{11}$, $G\alpha_{i2-3}$, $G\beta_1$, $G\beta_4$ and $G\gamma2$ were found to be localized at the mitochondria in the work reported here. Thus, taken together, this amounts to strong support for the mitochondrial localization of heterotrimeric G proteins. Although the mitochondrial targeting signal of the $G\alpha$ subunits is located in the N-terminus (124 aa) and this is sufficient to confer mitochondrial location, we show that the binding to $G\beta\gamma$ [57] provide further support for this targeting. Taking into account that WD-propeller proteins cannot cross through the TOM complex [58] and that we and others [4] found $G\beta\gamma$ located at the outer membrane, it seems that only the $G\alpha$ subunits can cross this membrane. At least for $G\alpha_q$, its dual location may be necessary for the coordination of the fusion of both the outer and the inner mitochondrial membrane. Both $G\alpha_{12}$ [2] and $G\alpha_q$ bind to the chaperon protein Hsp90 (unpublished results) and it is known that $G\alpha_{12}$ requires Hsp90 for mitochondrial targeting [2]. It is most likely that chaperone proteins are involved in the unfolding process necessary for crossing through the TOM complex [59]. So far we have not detected any proteolytic cleavage of $G\alpha_q$. So, the mechanism of entry of the $G\alpha$ subunits is still unclear and will require further research.

The mechanism of activation and the effectors downstream of the mitochondrial-located G proteins are still unknown. However, recent reports localized two different GPCRs at this organelle: the CB_1 receptor, found at the outer mitochondrial membrane of neurons [60]; and a functional angiotensin system at the inner membrane [61]. Those authors demonstrate that Ang II type 1 and 2 receptors are present in this subcompartment of the mitochondria and that the activation of the

mitochondrial angiotensin system is coupled to nitric oxide production which alters the respiratory capacity. These findings raise the possibility that GPCRs located at the mitochondria could couple to the G proteins also located at this organelle. The presence at the mitochondria of G protein-effectors or binding partners such as MAPKs, Akt, GRK2 and PKC [5,6] also supports the signaling of G proteins at mitochondria. However, the fact that the $G\beta_2$ subunit [4] binds directly to an intrinsic mitochondrial protein such as mitofusin 1, raises the possibility that mitochondrial proteins may act as receptor/effectors for a new non-canonical G protein effect.

$G\alpha_{q/11}$-depleted cells presented mitochondrial fragmentation and alterations in cristae; conversely, increases in $G\alpha_q$ levels elongate mitochondria. These alterations are reminiscent of those found in cells depleted in Mfns1–2 [49] and OPA1 [62]. Meanwhile, expression of Mfns1–2 or $G\beta\gamma$ leads to the formation of clusters of mitochondria due to outer membrane fusion [4,63], these clusters are not present when $G\alpha_q$ is co-expressed. We propose a mechanism in which $G\alpha_q$ and $G\beta\gamma$ are necessary for mitochondrial fusion via the coordinated regulation of the Mfn1 protein. However, mitochondria elongation can also be the result of inhibition of fission. It is particularly interesting that $G\alpha_q$ expression reduces Drp1 function. The Drp1 protein is recruited from the cytoplasm to the outer mitochondrial membrane where it forms assemblies and tubule constrictions around the organelle and, consequently, produces fission. Drp1 is posttranslationally modified by a variety of enzymes (phosphorylation, sumoylation, ubiquitination, S-nitrosylation), which highlights its complex regulation [64]. Our findings demonstrate that $G\alpha_q$ regulates mitochondrial morphology and respiratory efficiency through Mfn1 and Drp1-dependent mechanisms.

Mitochondrial fusion involves the coordination of both the outer and inner membranes [33,64]. Our results suggest that $G\alpha_{q/11}$ can also impinge on the inner membrane and crest morphology. $G\alpha_{q/11}$ effects could be explained by the altered processing of OPA1. Post-transcriptional regulation of OPA1 is rather complex, added to constitutive processing by different proteases (i-AAA, m-AAA and Parl) [65], which generate long and short OPA1 isoforms, all of which are required for mitochondrial fusion. L- and S-forms of OPA1 (a–b and c–d–e, respectively) form oligomers and keep cristae junctions tightly closed, thereby preventing cytosolic release of cytochrome c [66]. Under conditions of mitochondrial membrane depolarization (or CCCP treatment), ATP deficiency or apoptosis, the L-OPA1 isoforms undergo inducible cleavage by OMA1 which generates S-OPA1 forms (d and e), resulting in mitochondrial fragmentation. It is interesting to note that $G\alpha_{q/11}$-depleted cells that have reduced ATP due to lower membrane potential and fragmentation show an increase in L-forms (band b) and also in S-forms (band e). The increase in band e could be related to the lower membrane potential and is in agreement with the fact that mitochondria are fragmented. The higher band b, however, can only be a consequence of $G\alpha_{q/11}$ altering OPA1 processing. We consider that the mechanism of action of $G\alpha_{q/11}$ does not directly inhibit OMA1 function, since $G\alpha_{q/11}$-depleted cells present an increase in band e. Therefore, we propose that $G\alpha_{q/11}$ affects the processing of OPA1 isoforms by altering membrane potential and inner membrane fusion processes.

Our data also indicate that $G\alpha_{q/11}$ is required to maintain the proper organization of the respiratory complexes. Elongated mitochondria have higher levels of the dimeric form of ATPase, associated with increased efficiency in ATP production [67]. The absence of $G\alpha_{q/11}$ reduces not only this dimeric form (CV) but it also provokes an important reduction in supercomplexes containing complex I [68,69]. A primary consequence of the alteration in mitochondrial elongation and cristae organization by the absence of $G\alpha_{q/11}$ was a decrease in energy transfer. These results confirm previous findings linking mitochondrial morphology and energy fluxes [70]. OPA1 regulates cristae shape, organization and dynamics [66,71] and has been shown to interact directly with OXPHOS complexes I, II and III but not IV [72]. More recently, the lack of OPA1 or its processing by specific proteases that induce cristae remodeling was shown to

consequently reduce the amount of both respiratory supercomplexes containing complex I and complex I-dependent respiration [73].

Under normal conditions, mitochondrial fusion and fission take place at a balanced rate and thus a relatively constant tubular morphology is maintained. However, perturbation of the fission/fusion balance has been found to be associated with numerous human diseases [33,74]. Our findings raise the possibility that the non-canonical mitochondrial-function of $G\alpha_q$ may also account for some of the known functions of $G\alpha_q$ otherwise attributed to other pathways. Particularly interesting is the fact that $G\alpha_q$ signaling is essential for cardiomyocyte hypertrophy and proliferation during development [75]. However, it is also linked to hypertrophy of the adult myocardium and subsequent heart failure [76] where mitochondria need to sustain a high-energy demand [77] to avoid cell death under pathological conditions [78]. Therefore, understanding the functional role of $G\alpha_q$ at the mitochondria may open up new approaches to therapeutic treatments for cardiac diseases as well as other diseases.

Supplementary data to this article can be found online at http://dx.doi.org/10.1016/j.cellsig.2014.01.009.

Acknowledgments

References

[1] T. Hewavitharana, P.B. Wedegaertner, Cell. Signal. 24 (1) (2012) 25–34.
[2] A.V. Andreeva, M.A. Kutuzov, T.A. Voyno-Yasenetskaya, FASEB J. 22 (8) (2008) 2821–2831.
[3] J.S. Lyssand, S.M. Bajjalieh, FEBS Lett. 581 (30) (2007) 5765–5768.
[4] J. Zhang, W. Liu, J. Liu, W. Xiao, L. Liu, C. Jiang, X. Sun, P. Liu, Y. Zhu, C. Zhang, Q. Chen, Nat. Commun. 1 (2010) 101.
[5] V.G. Antico Arciuch, Y. Alippe, M.C. Carreras, J.J. Poderoso, Adv. Drug Deliv. Rev. 61 (14) (2009) 1234–1249.
[6] A. Fusco, G. Santulli, D. Sorriento, E. Cipolletta, C. Garbi, G.W. Dorn II, B. Trimarco, A. Feliciello, G. Iaccarino, Cell. Signal. 24 (2) (2012) 468–475.
[7] J.R. Hepler, A.G. Gilman, Trends Biochem. Sci. 17 (10) (1992) 383–387.
[8] N. Mizuno, H. Itoh, Neurosignals 17 (1) (2009) 42–54.
[9] P. Sengupta, F. Philip, S. Scarlata, J. Cell Sci. 121 (Pt 9) (2008) 1363–1372.
[10] M.D. Rochdi, V. Watier, C. La Madeleine, H. Nakata, T. Kozasa, J.L. Parent, J. Biol. Chem. 277 (43) (2002) 40751–40759.
[11] K.D. Little, M.E. Hemler, C.S. Stipp, Mol. Biol. Cell 15 (5) (2004) 2375–2387.
[12] Y. Sugawara, H. Nishii, T. Takahashi, J. Yamauchi, N. Mizuno, K. Tago, H. Itoh, Cell. Signal. 19 (6) (2007) 1301–1308.
[13] G. Boulay, X. Zhu, M. Peyton, M. Jiang, R. Hurst, E. Stefani, L. Birnbaumer, J. Biol. Chem. 272 (47) (1997) 29672–29680.
[14] B. Sjogren, R.R. Neubig, Mol. Pharmacol. 78 (4) (2010) 550–557.
[15] J.R. Hepler, D.M. Berman, A.G. Gilman, T. Kozasa, Proc. Natl. Acad. Sci. U. S. A. 94 (2) (1997) 428–432.
[16] C.V. Carman, J.L. Parent, P.W. Day, A.N. Pronin, P.M. Sternweis, P.B. Wedegaertner, A.G. Gilman, J.L. Benovic, T. Kozasa, J. Biol. Chem. 274 (48) (1999) 34483–34492.
[17] H. Usui, M. Nishiyama, K. Moroi, T. Shibasaki, J. Zhou, J. Ishida, A. Fukamizu, T. Haga, S. Sekiya, S. Kimura, Int. J. Mol. Med. 5 (4) (2000) 335–340.
[18] K. Momotani, M.V. Artamonov, D. Utepbergenov, U. Derewenda, Z.S. Derewenda, A.V. Somlyo, Circ. Res. 109 (9) (2011) 993–1002.
[19] K. Bence, W. Ma, T. Kozasa, X.Y. Huang, Nature 389 (6648) (1997) 296–299.
[20] G. Garcia-Hoz, G. Sanchez-Fernandez, M.T. Diaz-Meco, J. Moscat, F. Mayor, C. Ribas, J. Biol. Chem. 285 (18) (2010) 13480–13489.
[21] G.G. Tall, A.M. Krumins, A.G. Gilman, J. Biol. Chem. 278 (10) (2003) 8356–8362.
[22] J.S. Popova, J.C. Garrison, S.G. Rhee, M.M. Rasenick, J. Biol. Chem. 272 (10) (1997) 6760–6765.
[23] T.G. Frey, C.A. Mannella, Trends Biochem. Sci. 25 (7) (2000) 319–324.
[24] D. Chan, S. Frank, M. Rojo, Cell Death Differ. 13 (4) (2006) 680–684.
[25] A.E. Frazier, C. Kiu, D. Stojanovski, N.J. Hoogenraad, M.T. Ryan, Biol. Chem. 387 (12) (2006) 1551–1558.
[26] S. Campello, L. Scorrano, EMBO Rep. 11 (9) (2010) 678–684.
[27] M. Liesa, M. Palacin, A. Zorzano, Physiol. Rev. 89 (3) (2009) 799–845.
[28] B. Westermann, Nat. Rev. Mol. Cell Biol. 11 (12) (2010) 872–884.
[29] T. Koshiba, S.A. Detmer, J.T. Kaiser, H. Chen, J.M. McCaffery, D.C. Chan, Science 305 (5685) (2004) 858–862.
[30] N. Ishihara, Y. Fujita, T. Oka, K. Mihara, EMBO J. 25 (13) (2006) 2966–2977.
[31] S. Cipolat, O. Martins de Brito, B. Dal Zilio, L. Scorrano, Proc. Natl. Acad. Sci. U. S. A. 101 (45) (2004) 15927–15932.
[32] F. Malka, O. Guillery, C. Cifuentes-Diaz, E. Guillou, P. Belenguer, A. Lombes, M. Rojo, EMBO Rep. 6 (9) (2005) 853–859.
[33] H. Chen, D.C. Chan, Hum. Mol. Genet. 14 (Spec No. 2) (2005) R283–R289.
[34] B.B. Johansson, L. Minsaas, A.M. Aragay, FEBS J. 272 (20) (2005) 5365–5377.
[35] M. Liesa, B. Borda-d'Agua, G. Medina-Gomez, C.J. Lelliott, J.C. Paz, M. Rojo, A. Vidal-Puig, A. Zorzano, PLoS One 3 (10) (2008) e3613.
[36] M. Karbowski, D. Arnoult, H. Chen, D.C. Chan, C.L. Smith, R.J. Youle, J. Cell Biol. 164 (4) (2004) 493–499.
[37] D.D. D'Angelo, Y. Sakata, J.N. Lorenz, G.P. Boivin, R.A. Walsh, S.B. Liggett, G.W. Dorn II, Proc. Natl. Acad. Sci. U. S. A. 94 (15) (1997) 8121–8126.
[38] C. Merkwirth, S. Dargazanli, T. Tatsuta, S. Geimer, B. Lower, F.T. Wunderlich, J.C. von Kleist-Retzow, A. Waisman, B. Westermann, T. Langer, Genes Dev. 22 (4) (2008) 476–488.
[39] R. Acin-Perez, E. Salazar, M. Kamenetsky, J. Buck, L.R. Levin, G. Manfredi, Cell Metab. 9 (3) (2009) 265–276.
[40] M. Darshi, V.L. Mendiola, M.R. Mackey, A.N. Murphy, A. Koller, G.A. Perkins, M.H. Ellisman, S.S. Taylor, J. Biol. Chem. 286 (4) (2011) 2918–2932.
[41] S.V. Costes, D. Daelemans, E.H. Cho, Z. Dobbin, G. Pavlakis, S. Lockett, Biophys. J. 86 (6) (2004) 3993–4003.
[42] H. Schagger, Methods Enzymol. 260 (1995) 190–202.
[43] D.J. Pagliarini, S.E. Calvo, B. Chang, S.A. Sheth, S.B. Vafai, S.E. Ong, G.A. Walford, C. Sugiana, A. Boneh, W.K. Chen, D.E. Hill, M. Vidal, J.G. Evans, D.R. Thorburn, S.A. Carr, V.K. Mootha, Cell 134 (1) (2008) 112–123.
[44] A. Bhatnagar, D.J. Sheffler, W.K. Kroeze, B. Compton-Toth, B.L. Roth, J. Biol. Chem. 279 (33) (2004) 34614–34623.
[45] W.P. Li, P. Liu, B.K. Pilcher, R.G. Anderson, J. Cell Sci. 114 (Pt 7) (2001) 1397–1408.
[46] D.F. Dai, S.C. Johnson, J.J. Villarin, M.T. Chin, M. Nieves-Cintron, T. Chen, D.J. Marcinek, G.W. Dorn II, Y.J. Kang, T.A. Prolla, L.F. Santana, P.S. Rabinovitch, Circ. Res. 108 (7) (2011) 837–846.
[47] D.S. Evanko, M.M. Thiyagarajan, P.B. Wedegaertner, J. Biol. Chem. 275 (2) (2000) 1327–1336.
[48] S. Cipolat, T. Rudka, D. Hartmann, V. Costa, L. Serneels, K. Craessaerts, K. Metzger, C. Frezza, W. Annaert, L. D'Adamio, C. Derks, T. Dejaegere, L. Pellegrini, R. D'Hooge, L. Scorrano, B. De Strooper, Cell 126 (1) (2006) 163–175.
[49] H. Chen, S.A. Detmer, A.J. Ewald, E.E. Griffin, S.E. Fraser, D.C. Chan, J. Cell Biol. 160 (2) (2003) 189–200.
[50] A. Santel, M.T. Fuller, J. Cell Sci. 114 (Pt 5) (2001) 867–874.
[51] L. Ercolani, J.L. Stow, J.F. Boyle, E.J. Holtzman, H. Lin, J.R. Grove, D.A. Ausiello, Proc. Natl. Acad. Sci. U. S. A. 87 (12) (1990) 4635–4639.
[52] A. Leyte, F.A. Barr, R.H. Kehlenbach, W.B. Huttner, EMBO J. 11 (13) (1992) 4795–4804.
[53] S.W. Pimplikar, K. Simons, Nature 362 (6419) (1993) 456–458.
[54] J.L. Stow, K. Heimann, Biochim. Biophys. Acta 1404 (1–2) (1998) 161–171.
[55] M. Sato, J.B. Blumer, V. Simon, S.M. Lanier, Annu. Rev. Pharmacol. Toxicol. 46 (2006) 151–187.
[56] M. Chisari, D.K. Saini, V. Kalyanaraman, N. Gautam, J. Biol. Chem. 282 (33) (2007) 24092–24098.
[57] M.D. Resh, Sci. STKE 2006 (359) (2006) re14.
[58] R.K. Dagda, C.A. Barwacz, J.T. Cribbs, S. Strack, J. Biol. Chem. 280 (29) (2005) 27375–27382.
[59] A. Chacinska, C.M. Koehler, D. Milenkovic, T. Lithgow, N. Pfanner, Cell 138 (4) (2009) 628–644.
[60] G. Benard, F. Massa, N. Puente, J. Lourenco, L. Bellocchio, E. Soria-Gomez, I. Matias, A. Delamarre, M. Metna-Laurent, A. Cannich, E. Hebert-Chatelain, C. Mulle, S. Ortega-Gutierrez, M. Martin-Fontecha, M. Klugmann, S. Guggenhuber, B. Lutz, J. Gertsch, F. Chaouloff, M.L. Lopez-Rodriguez, P. Grandes, R. Rossignol, G. Marsicano, Nat. Neurosci. 15 (4) (2012) 558–564.
[61] P.M. Abadir, D.B. Foster, M. Crow, C.A. Cooke, J.J. Rucker, A. Jain, B.J. Smith, T.N. Burks, R.D. Cohn, N.S. Fedarko, R.M. Carey, B. O'Rourke, J.D. Walston, Proc. Natl. Acad. Sci. U. S. A. 108 (36) (2011) 14849–14854.
[62] L. Griparic, N.N. van der Wel, I.J. Orozco, P.J. Peters, A.M. van der Bliek, J. Biol. Chem. 279 (18) (2004) 18792–18798.
[63] A. Santel, S. Frank, B. Gaume, M. Herrler, R.J. Youle, M.T. Fuller, J. Cell Sci. 116 (Pt 13) (2003) 2763–2774.
[64] H. Otera, K. Mihara, J. Biochem. 149 (3) (2011) 241–251.
[65] L. Scorrano, Eur. J. Clin. Invest. 43 (8) (2013) 886–893.
[66] C. Frezza, S. Cipolat, O. Martins de Brito, M. Micaroni, G.V. Beznoussenko, T. Rudka, D. Bartoli, R.S. Polishuck, N.N. Danial, B. De Strooper, L. Scorrano, Cell 126 (1) (2006) 177–189.
[67] M. Strauss, G. Hofhaus, R.R. Schroder, W. Kuhlbrandt, EMBO J. 27 (7) (2008) 1154–1160.
[68] R. Acin-Perez, M.P. Bayona-Bafaluy, P. Fernandez-Silva, R. Moreno-Loshuertos, A. Perez-Martos, C. Bruno, C.T. Moraes, J.A. Enriquez, Mol. Cell 13 (6) (2004) 805–815.
[69] R. Acin-Perez, P. Fernandez-Silva, M.L. Peleato, A. Perez-Martos, J.A. Enriquez, Mol. Cell 32 (4) (2008) 529–539.
[70] J. Piquereau, F. Caffin, M. Novotova, A. Prola, A. Garnier, P. Mateo, D. Fortin, H. Huynh le, V. Nicolas, M.V. Alavi, C. Brenner, R. Ventura-Clapier, V. Veksler, F. Joubert, Cardiovasc. Res. 94 (3) (2012) 408–417.

[71] S. Meeusen, R. DeVay, J. Block, A. Cassidy-Stone, S. Wayson, J.M. McCaffery, J. Nunnari, Cell 127 (2) (2006) 383–395.

[72] C. Zanna, A. Ghelli, A.M. Porcelli, M. Karbowski, R.J. Youle, S. Schimpf, B. Wissinger, M. Pinti, A. Cossarizza, S. Vidoni, M.L. Valentino, M. Rugolo, V. Carelli, Brain 131 (Pt 2) (2008) 352–367.

[73] S. Cogliati, C. Frezza, M.E. Soriano, T. Varanita, R. Quintana-Cabrera, M. Corrado, S. Cipolat, V. Costa, A. Casarin, L.C. Gomes, E. Perales-Clemente, L. Salviati, P. Fernandez-Silva, J.A. Enriquez, L. Scorrano, Cell 155 (1) (2013) 160–171.

[74] E. Bossy-Wetzel, M.J. Barsoum, A. Godzik, R. Schwarzenbacher, S.A. Lipton, Curr. Opin. Cell Biol. 15 (6) (2003) 706–716.

[75] S. Offermanns, L.P. Zhao, A. Gohla, I. Sarosi, M.I. Simon, T.M. Wilkie, EMBO J. 17 (15) (1998) 4304–4312.

[76] J.W. Adams, J.H. Brown, Oncogene 20 (13) (2001) 1626–1634.

[77] S. Miyamoto, A.N. Murphy, J.H. Brown, J. Bioenerg. Biomembr. 41 (2) (2009) 169–180.

[78] R. Zak, M. Rabinowitz, C. Rajamanickam, S. Merten, B. Kwiatkowska-Patzer, Basic Res. Cardiol. 75 (1) (1980) 171–178.

[79] G. Sánchez-Fernández, S. Cabezudo, C. García-Hoz, C. Benincá, A.M. Aragay, F. Mayor Jr, C. Ribas, Cell Signal. 26 (5) (2014 Jan 17) 833–848, http://dx.doi.org/10.1016/j.cellsig.2014.01.010 [Epub ahead of print] Review.